Applied Catalysis B: Environmental 200 (2017) 477–483

Contents lists available at ScienceDirect

Applied Catalysis B: Environmental

journal homepage: www.elsevier.com/locate/apcatb

Noble-metal-free cobalt phosphide modified carbon nitride: An efficient photocatalyst for hydrogen generation

Sha-Sha Yi, Jun-Min Yan*, Ba-Ri Wulan, Si-Jia Li, Kai-Hua Liu, Qing Jiang

Key Laboratory of Automobile Materials (Jilin University), Ministry of Education, Department of Materials Science and Engineering, Jilin University, Changchun,130022, China

ARTICLE INFO

Article history:
Received 7 June 2016
Received in revised form 22 July 2016
Accepted 25 July 2016
Available online 26 July 2016

Keywords:
$g\text{-}C_3N_4$
Photocatalyst
Hydrogen generation
Visible light

ABSTRACT

Photocatalytic hydrogen generation from water is an important solar-to-chemical conversion process, and is also a sustainable and environment-friendly generation approach for energy source of hydrogen. Herein, for the first time, we report the noble-metal-free $CoP/g\text{-}C_3N_4$ hybrid as a photocatalyst for the highly efficient hydrogen generation by water splitting under visible light irradiation, whose hydrogen generation rate is ~131 times higher than that of pure $g\text{-}C_3N_4$, and is even better than that of $Pt/g\text{-}C_3N_4$. Based on the detailed analyses of photoluminescence (PL) spectra, UV–vis diffuse reflectance spectroscopy (UV–vis DRS), photocurrent-time (*i-t*) curves, and electrochemical impedance spectroscopy (EIS) Nyquist plots, the reason for the high efficiency of $CoP/g\text{-}C_3N_4$ is found to be its good absorption ability of visible light, highly effective separation and low recombination rate of photo-generated electron-hole pairs due to the addition of CoP to $g\text{-}C_3N_4$.

1. Introduction

Direct harvesting inexhaustible solar energy and applying it on photocatalytic hydrogen generation from water splitting is a promising technology for providing clean and renewable energy source ever since the first discovery of this phenomenon by Honda and Fujishima [1–5]. Semiconductor-based photocatalysts for hydrogen generation systems have been extensively explored, including metal oxides, sulfides and nitrides, doped perovskites, etc [6–10].

Very recently, graphitic carbon nitride ($g\text{-}C_3N_4$), a novel stable polymer semiconductor, is found to be an attractive candidate for direct generation of hydrogen by using solar energy in water due to its high stability, specific planar structure, and appropriate band gap (E_g) of ~2.7 eV [11–17]. However, the inherently fast recombination of photo-generated electron-hole pairs of pristine $g\text{-}C_3N_4$ greatly restricts its practical applications. Thus, loading of an earth-abundant cocatalyst on pure $g\text{-}C_3N_4$ to achieve a high efficiency in spatial charge separation and low activation energy of the reaction is of both scientific and economic importance [18–22]. Hong et al. have reported that NiS is a good cocatalyst for $g\text{-}C_3N_4$ due to the easy electron transfer from excited $g\text{-}C_3N_4$ to NiS [20]. Hou et al. have elaborated an effective cocatalyst of MoS_2 for $g\text{-}C_3N_4$ owning to its layered structure that could be easily constructed with $g\text{-}C_3N_4$ to form a graphene-like hybrid with thin layered heterojunctions [22]. To date, although numerous active cocatalysts have been introduced into the photocatalytic reaction, the efficiency of photocatalytic hydrogen generation from water splitting on $g\text{-}C_3N_4$ still awaits further studies.

Metal phosphides, such as, Ni_2P, MoP, Cu_3P, and CoP, have been widely reported as the acid-compatible electrocatalysts for hydrogen evolution reaction (HER) due to their earth abundances, low over potentials, and high stabilities under acidic conditions [23–27]. Among these phosphide catalyst, CoP possesses the outstanding efficiency for the electrochemical HER [28–30]. Further considering its narrow E_g (~1.7 eV) [31], CoP may also act as a promising visible-light catalyst. However, there is scarce research on CoP in photocatalytic hydrogen generation reaction by far.

Herein, we first use CoP nanoparticles (NPs) as the noble-metal-free cocatalyst for $g\text{-}C_3N_4$ to form an effective photocatalyst for hydrogen generation from water splitting under visible light irradiation. The resultant $CoP/g\text{-}C_3N_4$ hybrid leads to the high hydrogen generation rate of 474.4 $\mu mol\ h^{-1}\ g^{-1}$, which is ~131 times higher than that of pure $g\text{-}C_3N_4$, and is even superior to $Pt/g\text{-}C_3N_4$. The good catalytic performance of $CoP/g\text{-}C_3N_4$ is resulted from its good absorption ability of visible light, highly effective separation and low recombination rate of photo-generated electron-hole pairs during the photocatalytic water splitting process.

* Corresponding author.
E-mail address: junminyan@jlu.edu.cn (J.-M. Yan).

http://dx.doi.org/10.1016/j.apcatb.2016.07.046
0926-3373/

2. Experimental methods

2.1. Chemicals

All chemicals (AR grade) in the experiments were used without any further purification. Urea (H_2NCONH_2), cobalt nitrate hexahydrate ($Co(NO_3)_2{\cdot}6H_2O$), sodium hypophosphite (NaH_2PO_2), sodium borohydride ($NaBH_4$), chloroplatinic acid hexahydrate ($H_2PtCl_6{\cdot}6H_2O$) were bought from Sinopharm Chemical Reagent Co., Ltd. Sodium hydroxide (NaOH) was purchased from Aladdin Reagent Co., Ltd. Triethanolamine (TEOA) and sodium sulfate (Na_2SO_4) were purchased from Beijing Chemical Works. Ultrapure water with a specific resistance of 18.2 MΩ cm was obtained by reverse osmosis followed by ion-exchange and filtration.

2.2. Preparation of graphitic carbon nitride (g-C_3N_4)

g-C_3N_4 was synthesized thermally by heating urea (10 g) at 550 °C for 3 h with a heating rate of 4.6 °C min^{-1} under ambient pressure in air [32]. And then, the as-obtained yellowish powder was collected and grinded to get the final specimen.

2.3. Preparation of CoP NPs

CoP NPs were synthesized as follows [33]: typically, aqueous solutions of $Co(NO_3)_2{\cdot}6H_2O$ (50 mL, 0.05 M) and NaOH (20 mL, 0.25 M) were mixed under magnetic stirring. After 2 h, the precipitates were separated, washed with distilled water and ethanol, and then dried in vacuum to obtain the $Co(OH)_2$ precursor. Subsequently, the mixture of $Co(OH)_2$ (0.05 g) and NaH_2PO_2 (0.25 g) were ground uniformly. After that, the specimen was annealed in Ar at 300 °C for 1 h at a ramping rate of 2 °C min^{-1}. Finally, the obtained black solid was collected and washed for several times with distilled water and ethanol, and dried in vacuum.

2.4. Preparation of CoP/g-C_3N_4 nanostructures

The CoP/g-C_3N_4 hybrids were prepared by simply grinding the as-prepared g-C_3N_4 and CoP with different weight percentage of CoP (0.125, 0.25, 0.5, 1 and 5 wt%) for 30 min. The resulted specimens were labeled as 0.125 wt% CoP/g-C_3N_4, 0.25 wt% CoP/g-C_3N_4, 0.5 wt% CoP/g-C_3N_4, 1 wt% CoP/g-C_3N_4, and 5 wt% CoP/g-C_3N_4, respectively.

2.5. Preparation of Pt/g-C_3N_4

The hybrid of Pt/g-C_3N_4 was synthesized by a simple $NaBH_4$ reduction method. 0.25 g of g-C_3N_4 together with 0.64 mL of H_2PtCl_6 aqueous solution (2.6 mg/mL) were first put into 25 mL of water, and subsequently ultrasonicated for 5 min. Thereafter, 0.3 g of $NaBH_4$ was quickly put into the above solution. After stirring for 2 h, the obtained precipitates were washed and dried to get 0.25 wt% Pt/g-C_3N_4.

2.6. Characterizations

The crystalline structure of the as-prepared specimens were characterized by powder X-ray diffraction (XRD) with a Rigaku D/Max-2550 diffractometer using Cu Kα radiation (λ = 1.54056 Å) at 50 kV and 200 mA in the 2θ range of 10–80° at a scanning rate of 10° min^{-1}. X-ray photoelectron spectroscopy (XPS) measurements were performed on a Thermo VG Scientific ESCALAB 250 spectrometer using monochromatized Al Ka excitation. Ultraviolet-visible diffuse reflectance spectra (UV–vis DRS) were recorded on dispersions using a UV–vis-NIR spectrophotometer (Shimadzu UV-3600) over the range of 300–800 nm. Transmission electron microscopy (TEM), energy-dispersive X-ray (EDX) spectroscopy, and scanning TEM (STEM)-EDX elemental mapping were achieved by a JEOL JEM-2010 microscope (accelerating voltage = 200 kV). Room temperature photoluminescence (PL) spectra with an excitation wavelength of 325 nm were measured on a RF-5301 (Shimadzu).

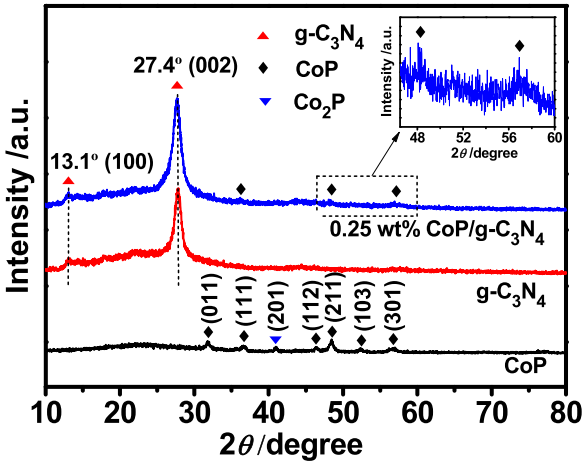

Fig. 1. XRD patterns of CoP, g-C_3N_4, and CoP/g-C_3N_4. Inset: the enlarged view of the circled area (for interpretation of the references to colour in the text, the reader is referred to the web version of this article).

Electrochemical and photoelectrochemical were tested by an electrochemical analyzer (CHI760E) in a three-electrode cell with the working electrodes of g-C_3N_4, CoP, and 0.25 wt% g-C_3N_4/CoP films on fluorine-doped tin oxide (FTO), the reference electrode of Ag/AgCl, and the counter electrode of Pt foil. Na_2SO_4 (0.5 M, pH = 7) solution was used as an electrolyte. A 300 W Xe lamp was applied as the simulated solar light (320 nm < λ < 2500 nm) source. The Mott-Schottky curves were performed under dark with a voltage of 5 mV at a frequency of 1 kHz. The photocurrent measurements were taken at an applied potential of 0.5 V vs Ag/AgCl under simulated solar light irradiation provided by a 300 W Xe lamp in 0.5 M Na_2SO_4 aqueous solution. The electrochemical impedance spectroscopy (EIS) was carried out in the frequency range from 0.01 to 100000 Hz with an AC voltage amplitude of 10 mV under open circuit potential conditions.

2.7. Photocatalytic hydrogen generation properties

Visible-light-driven hydrogen generation was performed with 0.1 g of photocatalyst suspended in triethanolamine aqueous solution (10 vol%, 100 mL) in a Pyrex glass reaction cell at 298 K under atmospheric pressure. A 300 W Xe lamp (CEL-HXF 300, 320 < λ < 2500 nm) with a UV cutoff filter (λ > 420 nm) was served as the visible-light source to trigger the photocatalytic reaction. The generated gas was analyzed by online gas chromatograph (GC-8A, Shimadzu Co., Japan, with N_2 as the carrier gas) equipped with a thermal conductivity detector (TCD).

3. Results and discussion

3.1. Structures and characterizations

Fig. 1 shows the XRD patterns of the as-prepared CoP, g-C_3N_4, and CoP/g-C_3N_4 for comparison. For specimen of pure CoP (Fig. 1, black trace), all peaks except one are indexed to be orthorhombic CoP phase (JCPDS No. 29-0497) [33], and the peak at 40.9° is corresponding to phase of Co_2P (JCPDS No. 32-0306) [34]. For specimen of pure g-C_3N_4 (Fig. 1, red trace), there are two characteristic diffraction peaks: the strong one at 27.4° is corresponded

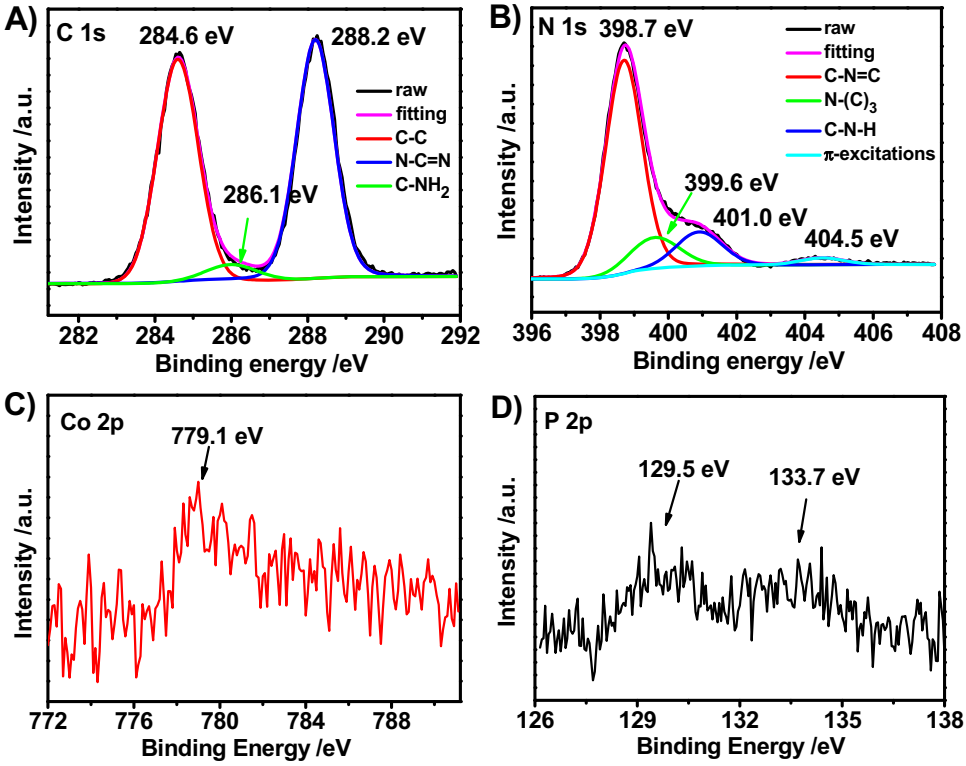

Fig. 2. XPS spectra of A) C 1s, B) N 1s, C) Co 2p, and D) P 2p in CoP/g-C_3N_4 (for interpretation of the references to colour in the text, the reader is referred to the web version of this article).

to the (002) peak with the interlayer d-spacing of 0.326 nm, and the weak one at 13.1° is attributed to (100) peak of in-planar structural packing motif with a distance of 0.675 nm (JCPDS No. 87-1526) [32,35–37]. The XRD pattern of the as-prepared CoP/g-C_3N_4 hybrid (0.25 wt% of CoP) proves that it contains phases of both CoP and g-C_3N_4 (Fig. 1 blue trace). The low diffraction intensities of CoP phase may result in its low content in the hybrid.

XPS is performed to investigate the surface chemical composition and valence state of CoP/g-C_3N_4 (1 wt% of CoP, the lower content of CoP in CoP/g-C_3N_4 will lead to the poor XPS signals for Co and P elements). The C 1s XPS spectrum (Fig. 2A) reveals that the characteristic C—C, N—C=N, and C—NH_2 species of g-C_3N_4 are presented at binding energies (BEs) of 284.6, 286.1 and 288.2 eV, respectively [37–39]. The N 1s XPS spectrum (Fig. 2B) proves the existences of C—N=C, N-$(C)_3$, C—N—H and π excitations of the C=N conjugated structures from g-C_3N_4, which are located at 398.7, 399.6, 401.0 and 404.5 eV, respectively [38–40]. The XPS spectra of Co 2p and P 2p (Fig. 2C and D) demonstrate that elements of Co and P are formed the phase of CoP, where the BE of Co 2p is located at 779.1 eV while P 2p has the two doublets with BE at 129.5 and 133.7 eV [41,42].

Furthermore, TEM and HRTEM are used to characterize the morphologies and structures of CoP/g-C_3N_4 (0.25 wt% of CoP) and pure g-C_3N_4. As shown in Fig. 3A, pure g-C_3N_4 has an irregular shape, a two-dimensional structure consisting of small thin flat sheets with wrinkles. Fig. 3B shows that, for specimen of CoP/g-C_3N_4, some particles are anchored on the surface of g-C_3N_4 with average size at around 25 nm. The HRTEM image taken from the nanoparticle (Fig. 3D) can be ascribed to the (201) diffraction plane of CoP with lattice spacing of 2.31 Å. EDX (Fig. 3C) and STEM-EDX elemental mapping (Fig. 3E) both confirms the existences of C, N, Co, and P elements as the XPS results. Moreover, the elemental mapping also demonstrates that CoP NPs are deposited on g-C_3N_4.

Normally, a high photocatalytic activity for a semiconductor is resulted from its good absorption of light, and efficient charge separation, and rapid transfer to the surface for redox reactions [18,43]. Fig. 4A displays the ultraviolet-visible diffuse reflectance spectra (UV–vis DRS) of g-C_3N_4 and CoP/g-C_3N_4 (0.25 wt% of CoP) specimens. As a result, after loading CoP on g-C_3N_4, an increase UV–vis light absorption over the entire wavelength range is discovered, demonstrating that CoP/g-C_3N_4 has the better UV–vis light absorption ability than pristine g-C_3N_4. To explore the separation of the photo-generated electron-hole pairs of the specimens, the photoluminescence (PL) measurement has been also applied. Fig. 4B shows the PL spectra of CoP/g-C_3N_4 (0.25 wt% of CoP) and g-C_3N_4 with their peaks both centered at ~460 nm. As a contrast, the intensity of PL emission peak for CoP/g-C_3N_4 is much weaker than that of g-C_3N_4, confirming the rapid charge transfer between g-C_3N_4 and CoP, namely, the high separation efficiency and low recombination of the photo-generated electron-hole pairs in hybrid of CoP/g-C_3N_4, and thus can leads to the enhancement of the photocatalytic activity [44].

Furthermore, the photocurrent-time (*i-t*) curves of CoP/g-C_3N_4 (0.25 wt% of CoP) and g-C_3N_4 working electrodes have been measured at 0.5 V vs. Ag/AgCl under simulated solar light irradiation. As shown in Fig. 4C, it is obviously that the photocurrent density for CoP/g-C_3N_4 is much higher than that of g-C_3N_4, suggesting a distinct improvement in the suppression of photo-generated electron-hole recombination [45,46], which is well consistent with the results of PL spectra (Fig. 4B). Moreover, there is no photocurrent density decay with the increased switch-on/off cycles, which means that the recombination of electron-hole is not occurred during the recycle application, that is to say, CoP/g-C_3N_4 has a good recycle stability [47]. Furthermore, electrochemical impedance spectroscopy (EIS) Nyquist plots are also performed to explore the advantage of CoP/g-C_3N_4 over g-C_3N_4 in the transport processes of photo-generated electron-hole pairs. A smaller arcs has been

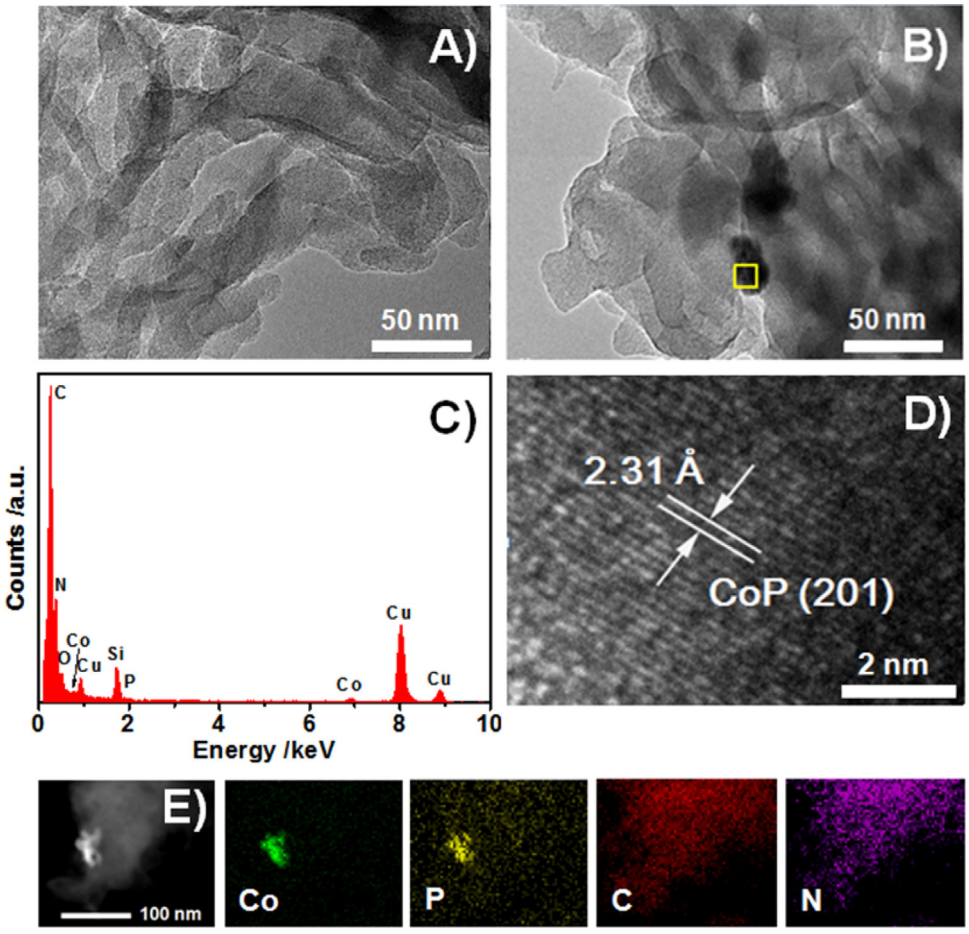

Fig. 3. A) TEM image of g-C_3N_4; B) TEM image, C) EDX spectrum, D) HRTEM image, and E) STEM-EDX elemental mapping for CoP/g-C_3N_4.

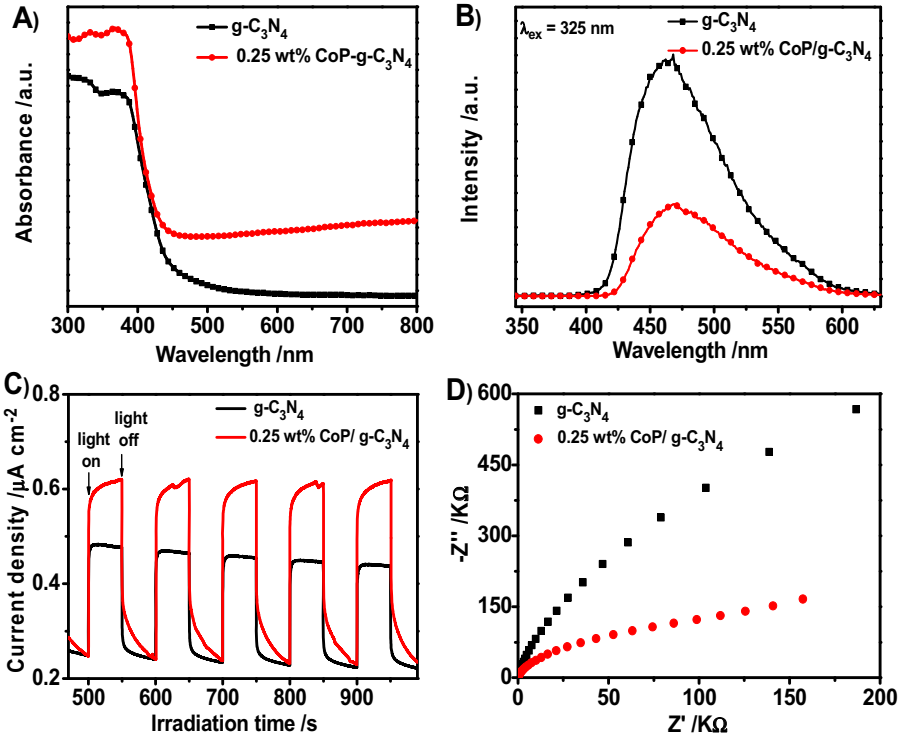

Fig. 4. A) UV–vis DRS for g-C_3N_4 and CoP/g-C_3N_4. B) PL spectra of g-C_3N_4 and CoP/g-C_3N_4 under an excitation wavelength of 325 nm. C) Transient photocurrent responses of g-C_3N_4 and CoP/g-C_3N_4 in 0.5 M Na_2SO_4 aqueous solution electrolyte at 0.5 V vs. Ag/AgCl under simulated solar light irradiation. D) Electrochemical impedance spectroscopy (EIS) Nyquist plots of g-C_3N_4 and CoP/g-C_3N_4 in darkness.

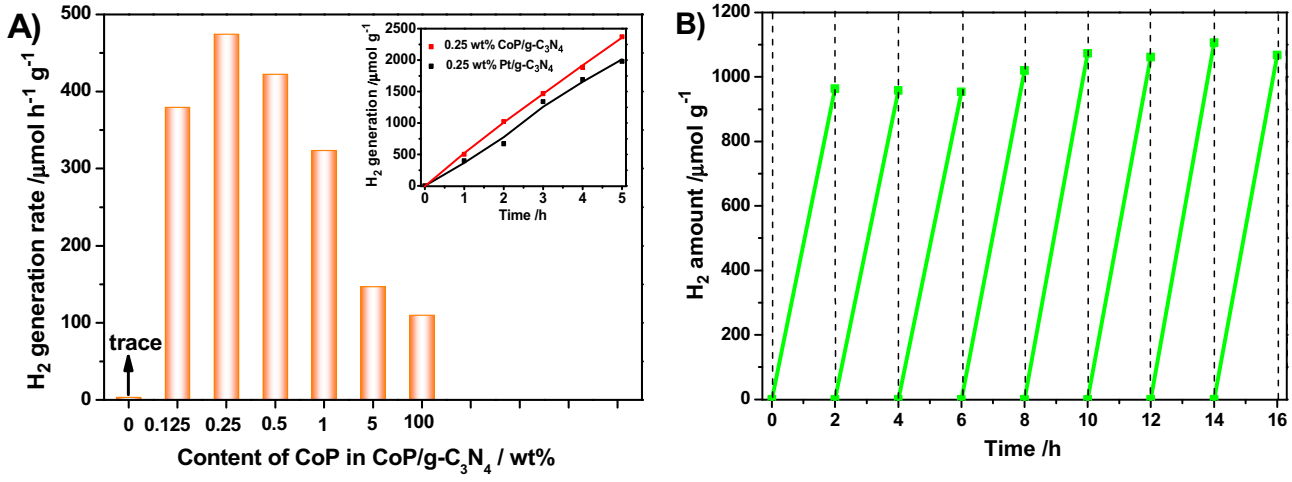

Fig. 5. A) Photocatalytic hydrogen generation rates over CoP/g-C_3N_4 hybrids with different contents of CoP (0, 0.125, 0.25, 0.5, 1, 5 and 100 wt%). B) Recycling test of photocatalytic activity of CoP/g-C_3N_4 (0.25 wt% of CoP). Inset: photocatalytic hydrogen generation rate vs. time over CoP/g-C_3N_4 (0.25 wt% of CoP) and Pt/g-C_3N_4 (0.25 wt% of Pt).

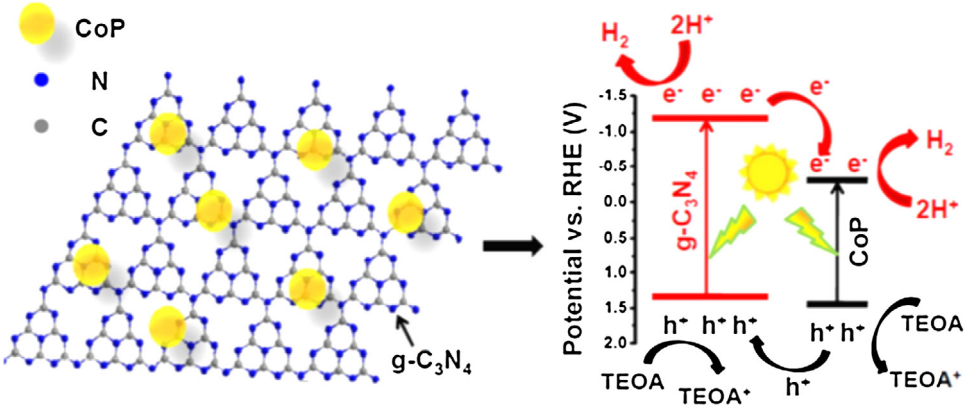

Scheme 1. Mechanism for photocatalytic hydrogen generation over CoP/g-C_3N_4.

observed for CoP/g-C_3N_4 as compared to that of g-C_3N_4 (Fig. 4D), which further proves the more effective charge separation and the faster charge transfer of CoP/g-C_3N_4 hybrid relative to pure g-C_3N_4 [48–50].

3.2. Photocatalytic hydrogen generation properties

The photocatalytic activities for hydrogen generation from water splitting over catalysts of CoP/g-C_3N_4 with different CoP contents together with pure g-C_3N_4 and CoP, are evaluated under visible light irradiation ($\lambda > 420$ nm) in the presence of triethanolamine as sacrificial electron donor. As shown in Fig. 5A, pure g-C_3N_4 shows a quite low photocatalytic activity (3.6 μmol h^{-1} g^{-1}) because of its low absorption of visible light and poor separation of photo-generated electrons and holes (Fig. 4) [19]. On the other hand, the pure CoP has a better but still very low activity (109 μmol h^{-1} g^{-1}). Interestingly, after adding a small amount of CoP into g-C_3N_4 (0.125 wt%), the activity of the CoP/g-C_3N_4 hybrid is remarkably enhanced. Especially when the loading amount of CoP is 0.25 wt%, the resultant CoP/g-C_3N_4 reaches the highest hydrogen generation activity (474.4 μmol h^{-1} g^{-1}), which is about 131 times higher than that of the pure g-C_3N_4. Moreover, the comparison of the photocatalytic hydrogen generation activities over CoP/g-C_3N_4 (0.25 wt% of CoP) and Pt/g-C_3N_4 (0.25 wt% of Pt) shows that CoP/g-C_3N_4 even demonstrates a higher activity than Pt/g-C_3N_4 (Fig. 5A, inset), indicating that noble-metal-free CoP can act as a quite better cocatalyst than noble Pt for g-C_3N_4.

The stability of CoP/g-C_3N_4 (0.25 wt% of CoP) is also carried out by the cycling hydrogen generation under a prolonged visible light irradiation of 16 h. As seen from Fig. 5B, the hydrogen generation rate shows no decrease after the recycle application, which means that CoP/g-C_3N_4 has a good photocatalytic stability. Moreover, the last cycle even higher than that of the first one because the hydrogen generation reaction is an activated process, and the photons absorbed on the surface of the photocatalyst are increased along with the irradiation time [51]. It is found that pure CoP has the better photocatalytic stability than that of pure g-C_3N_4 (Fig. S4). Therefore, the good stability of CoP/g-C_3N_4 may due to the addition of relatively stable CoP. Moreover, it is known that heteronanostructured photocatalysts with appropriate components can improve the separation of photo-generated electron-hole pairs by charge transfer [52], and thus, the good stability of CoP/g-C_3N_4 may also result from the timely charge transfer between CoP and g-C_3N_4 heterojunction (vide-infra).

3.3. Photocatalytic mechanism

To understand the enhancement of the photocatalytic hydrogen generation over CoP/g-C_3N_4, the positions of the lowest conduction band (E_{CB}) and the topmost valence band (E_{VB}) for the components

of CoP and g-C_3N_4 have been determined as follows. Based on the Tauc plots of $(\alpha h\nu)^n$ vs. photon energy ($h\nu$) and UV–vis absorption spectrum [53–55], the E_g of g-C_3N_4 and CoP are calculated to be 2.62 and 1.75 eV, respectively (Fig. S2), which is consistent well with the previous studies [11,12,31]. Mott-Schottky plots are under taken to determine the electronic band structures of both g-C_3N_4 and CoP (Fig. S3). Apparently, the positive slope of the Mott-Schottky plots are observed, which confirms the typical n-type characteristic of both g-C_3N_4 and CoP photocatalysts (Fig. S3) [56]. The flat band potentials for g-C_3N_4 and CoP are estimated to be −1.20 and −0.28 V vs. Ag/AgCl, respectively. Generally, the E_{CB} for n-type semiconductor is more negative about −0.1 or −0.2 V than its flat band potential [57], and thus, the CB potentials for g-C_3N_4 and CoP are roughly reckon up to be-1.40 and −0.48 V vs. Ag/AgCl, that is, −1.20 and −0.28 V vs. normal hydrogen electrode (NHE) ($E_{NHE} = E_{Ag/AgCl} + 0.197$ V) [58]. The E_{VB} for g-C_3N_4 and CoP are calculated to be 1.42 and 1.47 V vs. NHE by equation of $E_{VB} = E_{CB} + E_g$ [59], respectively. More clearly, the band positions of E_{CB} and E_{VB} for g-C_3N_4 and CoP are summarized in Table S1.

Therefore, the mechanism for photocatalytic hydrogen generation over CoP/g-C_3N_4 can be proposed based on the obtained band structures of CoP and g-C_3N_4 (Scheme 1). Under visible light illumination, g-C_3N_4 can be easily activated and generate electrons and holes. To some extent, CB-electrons of g-C_3N_4 can be quickly transferred to CB of CoP. And thus, CB-electrons of g-C_3N_4 together with the electrons accumulated on CoP can participate in the hydrogen generation reaction. Meanwhile, both the holes in the VB of g-C_3N_4 and CoP are scavenged by TEOA to oxidize $TEOA^+$. In such way, the whole process effectively suppresses the recombination of electron-hole pairs, resulting in the enhancement of the photocatalytic hydrogen generation. To sum up, there are two factors for the excellent performance of CoP/g-C_3N_4 hybrid on photocatalytic hydrogen generation: (1) CoP NPs serve as the good photosensitizer to enhance the visible light absorption; (2) CoP NPs also act as the electron acceptors from g-C_3N_4 to retard their recombination.

4. Conclusions

In conclusion, we have presented a novel noble-metal-free CoP modified g-C_3N_4, and the resultant CoP/g-C_3N_4 hybrid photocatalyst exhibits the high hydrogen generation rate from water splitting under visible light irradiation. Compared with the pristine g-C_3N_4, CoP/g-C_3N_4 hybrid shows a dramatically enhanced hydrogen generation activity, which is even higher than that of the optimized Pt/g-C_3N_4. The present good efficiency of CoP/g-C_3N_4 is highly depended on the addition of CoP, which greatly increases the visible light absorption, and leads to the high separation efficiency and low recombination rate of photo-generated electron-hole pairs.

Acknowledgements

This work is supported in part by the National Natural Science Foundation of China (51522101, 51471075, and 51401084); Scientific Research Foundation for Re-turned Overseas Chinese Scholars, Education of Ministry, China (3C1137282416); and Specialized Research Fund for the Doctoral Program of Higher Education of China (20110061120040).

Appendix A. Supplementary data

Supplementary data associated with this article can be found, in the online version, at http://dx.doi.org/10.1016/j.apcatb.2016.07.046.

References

[1] Q.J. Xiang, J.G. Yu, M. Jaroniec, Chem. Soc. Rev. 41 (2012) 782–796.
[2] Y. Tachibana, L. Vayssieres, J.R. Durrant, Nat. Photonics 6 (2012) 511–518.
[3] P.D. Tran, L.H. Wong, J. Barber, J.S.C. Loo, Energy Environ. Sci. 5 (2012) 5902–5918.
[4] Y. Ma, X.L. Wang, Y.S. Jia, X.B. Chen, H.X. Han, C. Li, Chem. Rev. 114 (2014) 9987–10043.
[5] A. Fujishima, K. Honda, Nature 238 (1972) 37–38.
[6] N. Nhat Truong, M. Altomare, J. Yoo, P. Schmuki, Adv. Mater. 27 (2015) 3208–3215.
[7] J.Q. Hu, A.L. Liu, H.L. Jin, D.K. Ma, D.W. Yin, P.S. Ling, S. Wang, Z.Q. Lin, J.C. Wang, J. Am. Chem. Soc. 137 (2015) 11004–11010.
[8] M.K. Bhunia, K. Yamauchi, K. Takanabe, Angew. Chem. Int. Ed. 53 (2014) 11001–11005.
[9] H.Q. Li, Y.X. Liu, X. Gao, C. Fu, X.C. Wang, ChemSusChem 8 (2015) 1189–1196.
[10] M. Wu, J.M. Yan, M. Zhao, Q. Jiang, ChemPlusChem 77 (2012) 931–935.
[11] M. Wu, J.M. Yan, X.N. Tang, M. Zhao, Q. Jiang, ChemSusChem 7 (2014) 2654–2658.
[12] M. Wu, J.M. Yan, X.W. Zhang, M. Zhao, Q. Jiang, J. Mater. Chem. A 3 (2015) 15710–15714.
[13] X.C. Wang, S. Blechert, M. Antonietti, ACS Catal. 2 (2012) 1596–1606.
[14] X.C. Wang, K. Maeda, A. Thomas, K. Takanabe, G. Xin, J.M. Carlsson, K. Domen, M. Antonietti, Nat. Mater. 8 (2009) 76–80.
[15] J.Q. Tian, Q. Liu, A.M. Asiri, A.O. Al-Youbi, X.P. Sun, Anal. Chem. 85 (2013) 5595–5599.
[16] J.Q. Tian, Q. Liu, A.M. Asiri, A.H. Qusti, A.O. Al-Youbi, X.P. Sun, Nanoscale 5 (2013) 11604–11609.
[17] J.Q. Tian, Q. Liu, A.M. Asiri, K.A. Alamry, X.P. Sun, ChemSusChem 7 (2014) 2125–2130.
[18] J.H. Yang, D.G. Wang, H.X. Han, C. Li, Acc. Chem. Res. 46 (2013) 1900–1909.
[19] S.W. Cao, J.X. Low, J.G. Yu, M. Jaroniec, Adv. Mater. 27 (2015) 2150–2176.
[20] J.D. Hong, Y.S. Wang, Y.B. Wang, W. Zhang, R. Xu, ChemSusChem 6 (2013) 2263–2268.
[21] J.G. Yu, S.H. Wang, B. Cheng, Z. Lin, F. Huang, Catal. Sci. Technol. 3 (2013) 1782–1789.
[22] Y.D. Hou, A.B. Laursen, J.S. Zhang, G.G. Zhang, Y.S. Zhu, X.C. Wang, S. Dahl, I. Chorkendorff, Angew. Chem. Int. Ed. 52 (2013) 3621–3625.
[23] J. Kibsgaard, T.F. Jaramillo, Angew. Chem. Int. Ed. 53 (2014) 14433–14437.
[24] T.Y. Wang, K.Z. Du, W.L. Liu, Z.W. Zhu, Y.H. Shao, M.X. Li, J. Mater. Chem. A 3 (2015) 4368–4373.
[25] E.J. Popczun, J.R. McKone, C.G. Read, A.J. Biacchi, A.M. Wiltrout, N.S. Lewis, R.E. Schaak, J. Am. Chem. Soc. 135 (2013) 9267–9270.
[26] J.F. Callejas, J.M. McEnaney, C.G. Read, J.C. Crompton, A.J. Biacchi, E.J. Popczun, T.R. Gordon, N.S. Lewis, R.E. Schaak, ACS Nano. 8 (2014) 11101–11107.
[27] J.Q. Tian, Q. Liu, N.Y. Cheng, A.M. Asiri, X.P. Sun, Angew. Chem. Int. Ed. 53 (2014) 9577–9581.
[28] J.Q. Tian, Q. Liu, A.M. Asiri, X.P. Sun, J. Am. Chem. Soc. 136 (2014) 7587–7590.
[29] Q. Liu, J.Q. Tian, W. Cui, P. Jiang, N.Y. Cheng, A.M. Asiri, X.P. Sun, Angew. Chem. Int. Ed. 53 (2014) 6710–6714.
[30] Z.H. Pu, Q. Liu, P. Jiang, A.M. Asiri, A.Y. Obaid, X.P. Sun, Chem. Mater. 26 (2014) 4326–4329.
[31] W. Maneeprakorn, M.A. Malik, P. O'Brien, J. Mater. Chem. 22 (2010) 2329–2335.
[32] Y.W. Zhang, J.H. Liu, G. Wu, W. Chen, Nanoscale 4 (2012) 5300–5303.
[33] S. Cao, Y. Chen, C.J. Wang, X.J. Lv, W.F. Fu, Chem. Commun. 51 (2015) 8708–8711.
[34] S. Cao, Y. Chen, C.C. Hou, X.J. Lv, W.F. Fu, J. Mater. Chem. A 3 (2015) 6096–6101.
[35] L. Ge, C.C. Han, J.K. Liu, J. Mater. Chem. 22 (2012) 11843–11850.
[36] L. Ge, F. Zuo, J.K. Liu, Q. Ma, C. Wang, D.Z. Sun, L. Bartels, P.Y. Feng, J. Phys. Chem. C 116 (2012) 13708–13714.
[37] S.W. Zhang, J.X. Li, M.Y. Zeng, J. Li, J.Z. Xu, X.K. Wang, Chem. Eur. J. 20 (2014) 9805–9812.
[38] Q.H. Liang, Z. Li, X.L. Yu, Z.H. Huang, F.Y. Kang, Q.H. Yang, Adv. Mater. 27 (2015) 4634–4639.
[39] T.Y. Ma, S. Dai, M. Jaroniec, S.Z. Qiao, Angew. Chem. Int. Ed. 53 (2014) 7281–7285.
[40] Z.Z. Lin, X.C. Wang, Angew. Chem. Int. Ed. 52 (2013) 1735–1738.
[41] X.L. Yang, A.Y. Lu, Y.H. Zhu, M.N. Hedhili, S.X. Min, K.W. Huang, Y. Han, L.J. Li, Nano Energy 15 (2015) 634–641.
[42] A. Infantes-Molina, J. Cecilia, B. Pawelec, J. Fierro, E. Rodríguez-Castellón, A. Jiménez López, Appl. Catal. A: Gen. 390 (2010) 253–263.
[43] F.Y. Wen, C. Li, Acc. Chem. Res. 46 (2013) 2355–2364.
[44] Z.J. Sun, X. Liu, Q.D. Yue, H.X. Jia, P.W. Du, ChemCatChem 8 (2016) 157–162.
[45] Y.H. Zhang, Z.R. Tang, X.Z. Fu, Y.J. Xu, ACS Nano. 5 (2011) 7426–7435.
[46] J. Zhang, L.F. Qi, J.R. Ran, J.G. Yu, S.Z. Qiao, Adv. Energy Mater. 4 (2014) 1301925–1301930.
[47] J. Zhang, J.G. Yu, M. Jaroniec, J.R. Gong, Nano Lett. 12 (2012) 4584–4589.
[48] N. Zhang, M.Q. Yang, Z.R. Tang, Y.J. Xu, ACS Nano. 8 (2014) 623–633.
[49] C. Han, Z. Chen, N. Zhang, J.C. Colmenares, Y.J. Xu, Adv. Funct. Mater. 25 (2015) 221–229.
[50] Y. Hou, F. Zuo, A.P. Dagg, J.K. Liu, P.Y. Feng, Adv. Mater. 26 (2014) 5043–5049.
[51] J.Y. Zhang, Y.H. Wang, J. Jin, J. Zhang, Z. Lin, F. Huang, J.G. Yu, ACS Appl. Mater. Interfaces 5 (2013) 10317–10324.

[52] Y.P. Yuan, L.W. Ruan, J. Barber, S.C.J. Loo, C. Xue, Energy Environ. Sci. 7 (2014) 3934–3951.
[53] M. Butler, J. Chem. Phys. 48 (1977) 1914–1920.
[54] J.S. Zhang, M.W. Zhang, C. Yang, X.C. Wang, Adv. Mater. 26 (2014) 4121–4126.
[55] S.B. Yang, Y.J. Gong, J.S. Zhang, L. Zhan, L.L. Ma, Z.Y. Fang, R. Vajtai, X.C. Wang, P.M. Ajayan, Adv. Mater. 25 (2013) 2452.
[56] A. Ishikawa, T. Takata, J.N. Kondo, M. Hara, H. Kobayashi, K. Domen, J. Am. Chem. Soc. 124 (2002) 13547–13553.
[57] X. Li, J.G. Yu, J.X. Low, Y.P. Fang, J. Xiao, X.B. Chen, J. Mater. Chem. A 3 (2015) 2485–2534.
[58] G. Ai, H.X. Li, S.P. Liu, R. Mo, J.X. Zhong, Adv. Funct. Mater. 25 (2015) 5706–5713.
[59] L.J. Zhang, S. Li, B.K. Liu, D.J. Wang, T.F. Xie, ACS Catal. 4 (2014) 3724–3729.